Biorheology 35:4,5 (1998) 281–294

Low Reynolds number turbulence modeling of blood flow in arterial stenoses

Farzan Ghalichi, *† Xiaoyan Deng, † Alain De Champlain, * Yvan Douville, † Martin King, † and Robert Guidoin †

* *Department of Mechanical Engineering, Laval University, and Québec Biomaterials Institute, Inc., Pavillon St-François d'Assise, CHUQ, Québec, Qc, Canada, G1L 3L5*
† *Department of Surgery, Laval University, and Québec Biomaterials Institute, Inc., Pavillon St-François d'Assise, CHUQ, Québec, Qc, Canada, G1L 3L5*

Received 29 December 1997; accepted in revised form 13 November 1998

Abstract

Moderate and severe arterial stenoses can produce highly disturbed flow regions with transitional and or turbulent flow characteristics. Neither laminar flow modeling nor standard two-equation models such as the k-ε turbulence ones are suitable for this kind of blood flow. In order to analyze the transitional or turbulent flow distal to an arterial stenosis, authors of this study have used the Wilcox low-*Re* turbulence model. Flow simulations were carried out on stenoses with 50, 75 and 86% reductions in cross-sectional area over a range of physiologically relevant Reynolds numbers. The results obtained with this low-*Re* turbulence model were compared with experimental measurements and with the results obtained by the standard k-ε model in terms of velocity profile, vortex length, wall shear stress, wall static pressure, and turbulence intensity. The comparisons show that results predicted by the low-*Re* model are in good agreement with the experimental measurements. This model accurately predicts the critical Reynolds number at which blood flow becomes transitional or turbulent distal an arterial stenosis. Most interestingly, over the *Re* range of laminar flow, the vortex length calculated with the low-*Re* model also closely matches the vortex length predicted by laminar flow modeling. In conclusion, the study strongly suggests that the proposed model is suitable for blood flow studies in certain areas of the arterial tree where both laminar and transitional/turbulent flows coexist.

Keywords: Turbulent flow; numerical modeling; hemodynamics; wall shear stress

Reprint requests to: Dr Robert Guidoin, Laboratory of Experimental Surgery, Room 1701 Services Building, Laval University, Sainte-Foy, PQ, Canada G1K 7P4; Tel.: (418) 656-2621; Fax: (418) 656-7512; e-mail: x.deng@crsfa.ulaval.ca

1. Introduction

The accumulation of cholesterol and the proliferation of connective tissue in an arterial wall lead to the formation of plaques which grow inward and restrict blood flow. Once the local constriction or stenosis becomes large enough to produce a flow separation zone, it is possible that further and possibly more rapid growth of the stenosis can be induced by this flow pattern.

Moderate and severe stenoses may lead to a highly disturbed flow region downstream of the stenosis. These disturbed flows may either remain laminar or may undergo transition to turbulent flow, depending upon the flow rate through the stenosis and the geometry of the stenosis. The development of turbulent flow has important clinical consequences, as turbulence represents an abnormal flow condition in the circulation and is related to several vascular disorders such as post-stenotic dilatation (Boughner and Roach, 1971; Cassanova and Giddens, 1978). It may also lead to significant losses in pressure and abnormally high shear stresses, which may result in hemolysis and the activation of platelets.

The occurrence of turbulence in stenotic regions has long been recognized (Roach, 1972). Since then, numerous experimental studies have been carried out in animals (Giddens et al., 1976), in stenosis models (Clark, 1976; Saad and Giddens, 1983), and in humans (Strandness et al., 1987). These studies have shown that, even with relatively mild stenoses, transitional flow or turbulence can be expected distal to the constriction (Clark, 1980; Saad and Giddens, 1983). Numerical simulation of blood flow offers a noninvasive means of obtaining detailed flow patterns, such as wall shear stress distributions, which are very difficult to obtain experimentally. Unfortunately, most numerical modeling of stenotic flow has been limited to laminar flow models with low Reynolds numbers (Lee and Fung, 1970; Daly, 1976; Deshpande et al., 1976). In another study Deshpande (1977) did predict turbulent flow in arterial stenoses, but the Reynolds number that was used was as high as 15,000, which is certainly unrealistic when considering the human circulatory system.

In the present study, we planned to simulate blood flow in arterial stenoses using the Wilcox low-*Re* k-ω turbulence model (Wilcox, 1993). To validate this model we planned to compare our numerical analysis with previously reported experimental results (Deshpande and Giddens, 1980; Saad and Giddens, 1983) and with published numerical predictions obtained from the standard k-ε turbulence flow model and laminar flow modeling methods.

2. Method

2.1. Assumptions

To simplify the analysis, the following assumptions were made: (1) The fluid (blood) is homogeneous, incompressible, and Newtonian, with a constant kinematic viscosity of 0.035 cm^2/sec and a mass density of 1.06 g/cm^3; (2) The flow is steady and axisymmetric. The steady flow assumption is fairly realistic for large arteries which experience a relatively constant forward flow during diastole, which occupies approximately two-thirds of the cardiac cycle; (3) In the range of *Re* studied, the flow proximal to the stenoses remains relatively laminar; and (4) The form of the stenoses chosen for this study is $r(z)/D = 0.5 - A[1 + \cos \pi z/D]$, $-D \leqslant z \leqslant D$, with $z = 0$ at the throat of the stenosis (Fig. 1) and D is the upstream

artery diameter which is taken 1 in nondimensional form by assuming D as a reference length in nondimensionalizing.

In this study, three stenosis models were considered. Model 1 has a constriction with a lumen area reduction of 50% ($A = 0.073$) giving $r = 0.354$ at the throat. Model 2 has a more severe stenosis with an area reduction of 75% ($A = 0.125$) giving $r = 0.25$ at the throat, whereas Model 3 has an even more severe condition of 86% ($A = 0.1565$) and $r = 0.187$. The percentage of stenosis is defined as $[1 - (r/R)^2]$, where r and R are the throat and upstream arterial radii, respectively. A parabolic velocity profile was imposed at the inflow which is located 15 diameters (D) prior to the stenosis, to ensure full development of the upstream flow, where D is the unobstructed arterial diameter. The outflow boundary condition was located 20 diameters (D) downstream of the stenosis throat to allow for the redevelopment of flow.

2.2. Basic equations

In the present study, we focused our numerical modeling on blood flows with moderate Reynolds numbers ranging from 400 (in the human common carotid artery) to 1,500 (in the human ascending aorta). In this range of Reynolds numbers, the viscous sub-layer is usually much thicker than found at higher Reynolds numbers with turbulent flow.

Standard k-ε equations were not considered suitable for the present study, because these equations are unreliable for predicting separated flows (Wilcox, 1993). We therefore chose the Wilcox low-*Re* k-ω turbulence model (k and ω are the turbulent kinetic energy and specific dissipation rate proportional to ε/k, respectively) (Wilcox, 1993) for our simulation. An important advantage of this model is that it can be used to directly predict low-*Re* effects on the turbulence field in the near-wall regions (FIDAP Update Manual, 1995) and has been proven to be more accurate in describing the transition from laminar to turbulent flow (FIDAP Update Manual, 1995). This model was designed originally with the primary intention of simulating global low-Reynolds flows where $Re \leqslant 10{,}000$, but it can also be used to predict high Reynolds internal flows. This, however, will typically require a significantly large number of grid points compared to a k-ε type simulation using the specialized near-wall model. The k-ω model can also be used in conjunction with a fine near-wall mesh to model both the mean flow variables and the turbulence variables close to the wall and resolve any geometric feature which may be present in the viscous sublayer.

The steady-state mean flow equations, transport equations for k and ω in the Wilcox model and the continuity equations were defined as follows:

$$\rho_0 u_j \cdot u_{i,j} = -p_{,i} + \left[\mu(u_{i,j} + u_{j,i})_{,j}\right], \tag{1}$$

$$\rho u_j \frac{\partial k}{\partial x_j} = \frac{\partial}{\partial x_j}\left[\left(\mu + \frac{\mu_t}{\sigma_k}\right)\frac{\partial k}{\partial x_j}\right] + G - \rho\omega k, \tag{2}$$

$$\rho u_j \frac{\partial \omega}{\partial x_j} = \frac{\partial}{\partial x_j}\left[\left(\mu + \frac{\mu_t}{\sigma_\omega}\right)\frac{\partial \omega}{\partial x_j}\right] + c_1\frac{\omega}{k}G - c_2\rho\omega^2, \tag{3}$$

$$u_{j,j} = 0, \quad \text{i.e.,} \quad \frac{\partial u}{\partial x} + \frac{\partial v}{\partial y} + \frac{\partial w}{\partial z} = 0, \tag{4}$$

where the turbulent viscosity

$$\mu_t = c_\mu \rho \frac{k}{\omega},$$

and the generation rate of turbulence kinetic energy

$$G = \mu_t \left(\frac{\partial u_i}{\partial x_j} + \frac{\partial u_j}{\partial x_i} \right) \frac{\partial u_i}{\partial x_j}.$$

The values of the Wilcox model constants were:

$$c_1 = 0.555, \quad c_2 = 0.8333, \quad c_\mu = 0.09, \quad \sigma_k = 2, \quad \sigma_\omega = 2.$$

2.3. Boundary conditions

The boundary conditions were:

$$u_z = U\left[1 - \left(\frac{r}{R}\right)^2\right], \quad u_r = 0, \quad \text{at the inlet (assumption 3)}, \tag{5}$$

$$\frac{\partial u_z}{\partial r} = u_r = 0, \quad \text{at the axis of the vessel}, \tag{6}$$

$$u_z = u_r = 0, \quad \text{at the wall of the vessel}. \tag{7}$$

At the vessel outlet, normal and tangential stresses were set at zero (FIDAP Tutorial Manual, 1995). The boundary conditions for the k-ω model at the non-slip wall were

$$k = 0 \quad \text{and} \quad \omega = \frac{6\mu}{c_2 \Delta^2}, \tag{8}$$

where Δ is the height of the first node above the wall. The boundary condition for k was applied at the wall, whereas that for ω was at the first node above the wall. At the inlet of the vessel, assuming that the flow is laminar, in nondimensional form k and ω were set at very low levels (FIDAP Tutorial Manual, 1995):

$$k = 0.0001, \quad \omega = 0.45 \quad (\varepsilon = 0.000045). \tag{9}$$

At the outlet, it was assumed that the flow was fully developed, and the properties no longer varied with the distance along the vessel (FIDAP Tutorial Manual, 1995), i.e.,

$$\frac{\partial k}{\partial z} = \frac{\partial \omega}{\partial z} = 0. \tag{10}$$

2.4. Numerical approach

Equations (1)–(3) (with the proper boundary conditions stated above) were solved using the FIDAP (Fluid Dynamic Analysis Package) finite element software. A staged grid system was used in the numerical simulation and is shown in Fig. 1. After grid dependence tests, a 290×30 cell mesh system was chosen to carry out the numerical simulations in the arterial stenosis models at Reynolds numbers up to 2,000. The Reynolds number, Re, is defined as $Re = \rho U_m D/\mu$, in which U_m is the flow mean velocity, D is the normal artery diameter and μ is the constant dynamic viscosity. In the core flow region, nine node isoparametric

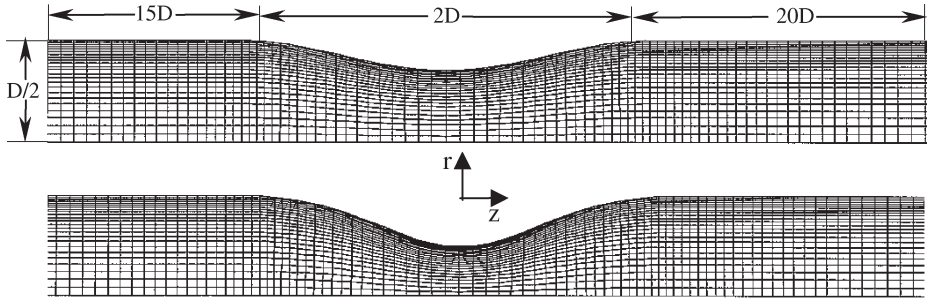

$$r(z)/D = 0.5 - A\,[1 + \cos \pi z/D]$$

Fig. 1. Geometry of the stenosis model and the grid system for the arterial stenosis flow.

quadrilateral elements were employed. A single layer of specialized near-wall elements was used to capture the low-*Re* effects on the turbulence field in the near-wall region. The thickness of this special element was chosen to fully contain the viscous sublayers and to resolve any geometric feature present in the viscous sublayers (FIDAP Update Manual, 1995). For an optimum result, the first grid point above the wall was given a value of $y^+ \leqslant 1$, where $y^+ = \mu_\tau y/\upsilon$ is the sublayer-scaled distance.

The k-ω turbulence model does have some limitations. Although, the low-Reynolds-number version of this model can accurately predict the minimum critical Reynolds number for the Blasius (flat-plate) boundary layer, in general, it must be recalibrated for each new application as the model does not include sufficient physics to accurately predict any transitions in flow.

3. Results

3.1. Validation of the numerical method

To verify the accuracy of the calculations, the numerical results were compared with the experimental data published by Saad and Giddens (1983) in terms of axial velocity profiles (Figs 2A and 2B) and wall shear stresses at the constriction (Fig. 2C). The comparison shows that the predicted velocity profiles are in good agreement with the experimental measurements. However, the predicted wall shear stress at the throat is approximately 40% higher than the reported experimental results. It should be noted that the wall shear stress values at the stenotic throat given by Saad and Giddens (1983) are estimations from velocity measurements at three stations at a certain distance away from the wall. Since the value of wall shear stress is very sensitive to the velocity profile near the wall, the data by Saad and Giddens (1983) is likely an underestimate of the true wall shear stress at the throat.

3.2. Streamlines and vortex length

Figure 3 presents typical streamlines in the first two stenosis models. In Fig. 4, the vortex length, is plotted in nondimensional form (L_a/D) as a function of the Reynolds number. The flow simulations for stenoses of 50% or greater show that the vortex length increases almost linearly with *Re* until it reaches a critical peak value. This indicates that flow distal

(A)

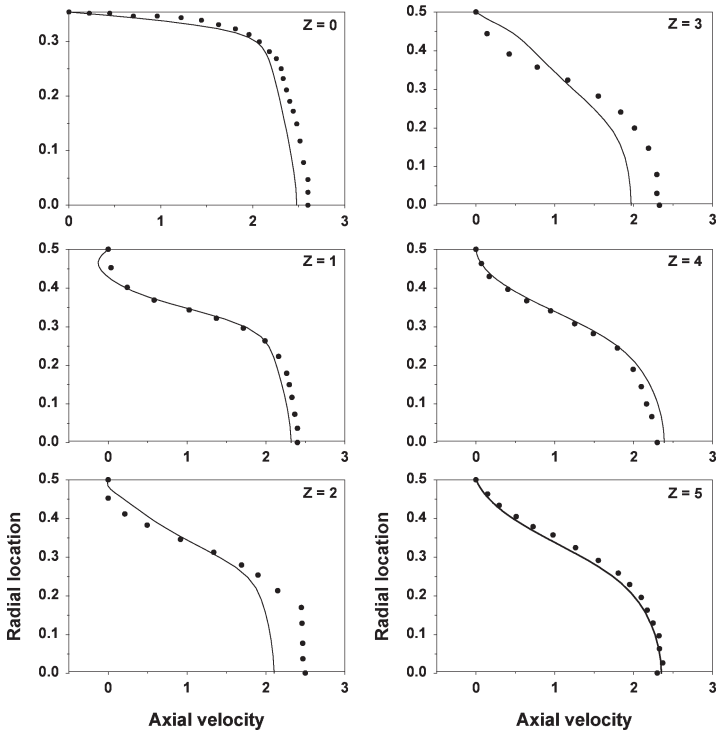
Z = 0
Z = 3
Z = 1
Z = 4
Z = 2
Z = 5
Radial location
Axial velocity

(B)

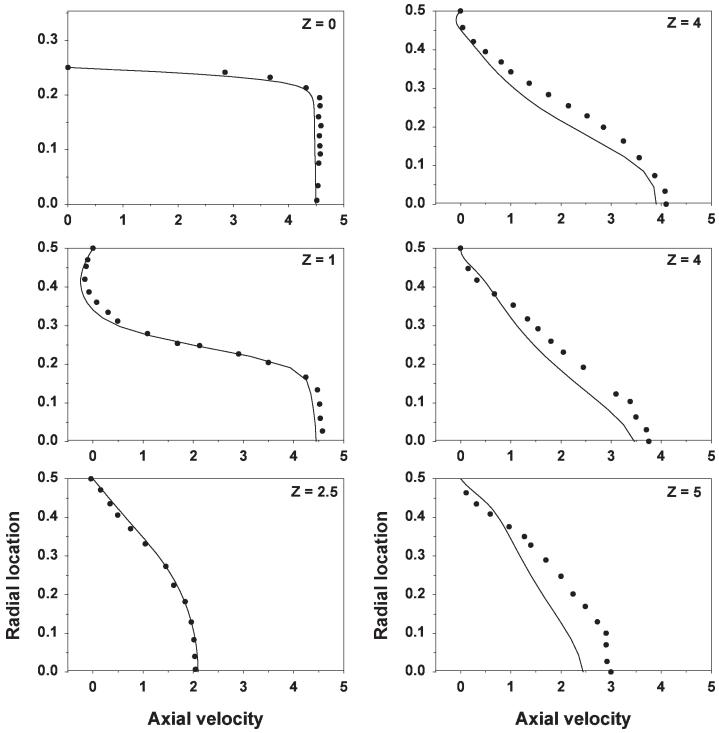
Z = 0
Z = 4
Z = 1
Z = 4
Z = 2.5
Z = 5
Radial location
Axial velocity

(C)

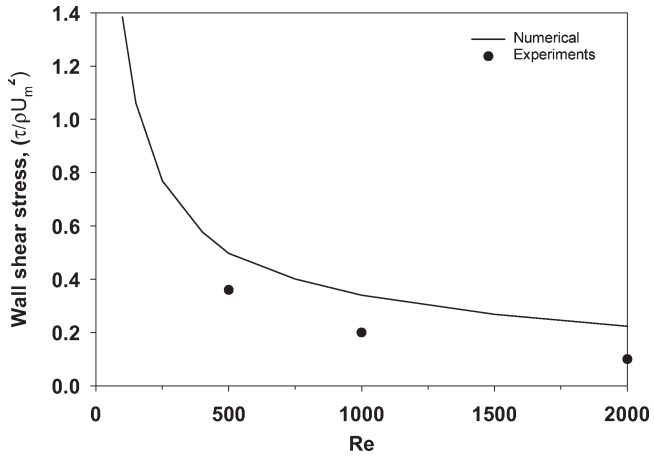

Fig. 2. Comparison of the numerical results by the low-*Re* model with experimental measurements. (A) Axial velocity profiles at different axial locations in a 50% stenosis, $Re = 1{,}000$. The curves are numerical results, dots: experimental data; (B) Axial velocity profiles at different axial locations in a 75% stenosis, $Re = 500$. The curves are numerical results, dots: experimental results; (C) Wall shear stress at the stenotic throat as a function of Reynolds number. All the experimental measurements originated from Saad and Giddens (1983).

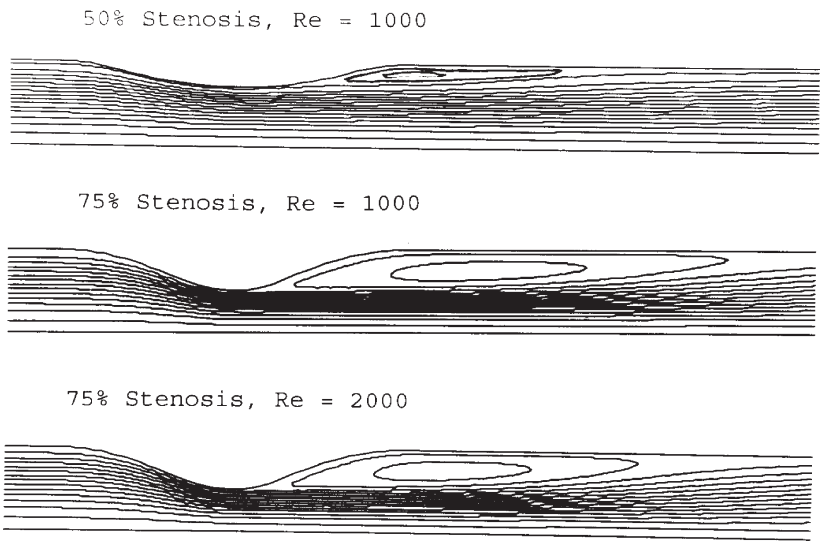

Fig. 3. Typical streamlines for 50 and 75% stenoses, showing the effect of Reynolds numbers on vortex length.

to the stenosis is in a state of laminar flow when the Reynolds number is below its critical value, and it becomes transitional or turbulent when the *Re* was larger than the critical value. Numerical modeling with the low-*Re* model predicts that the critical Reynolds number is approximately 1,100 for Model 1 and 400 for Model 2, which are values that lie within 10%

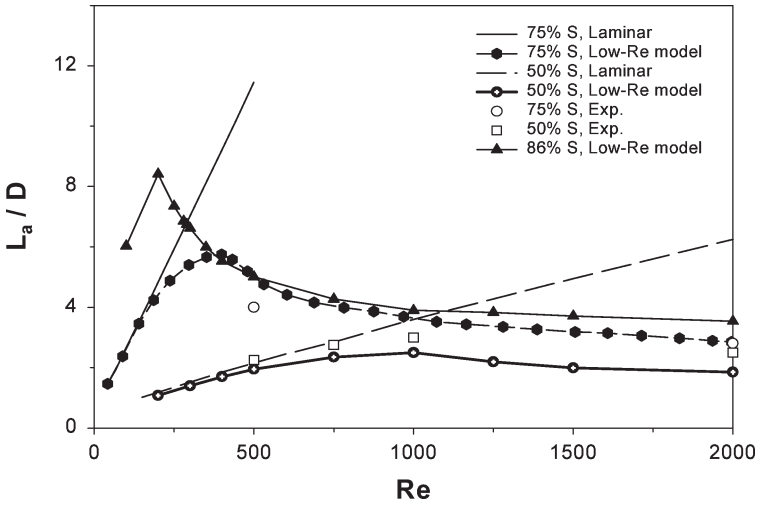

Fig. 4. Plots of vortex length as a function of Reynolds number. Exp.: Experimental measurements (Saad and Giddens, 1983); Low-*Re* model: Low-*Re* turbulence model prediction; Laminar: Laminar flow model prediction.

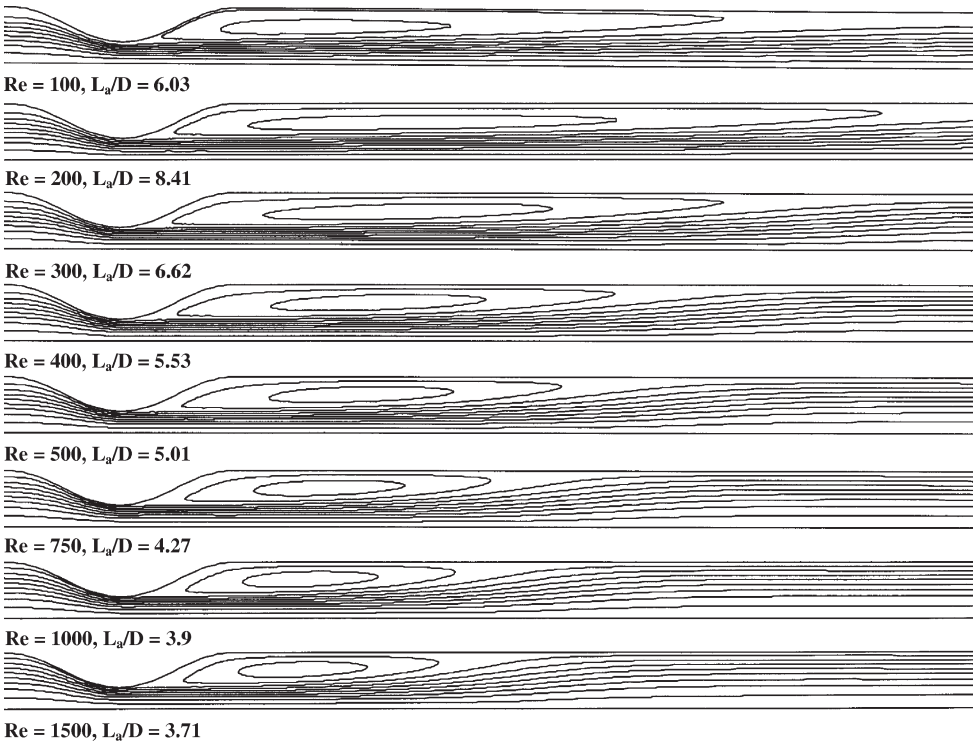

Fig. 5. Variations in vortex length with different Reynolds numbers in a 86% stenosis, predicted by the Wilcox low-*Re* turbulence model.

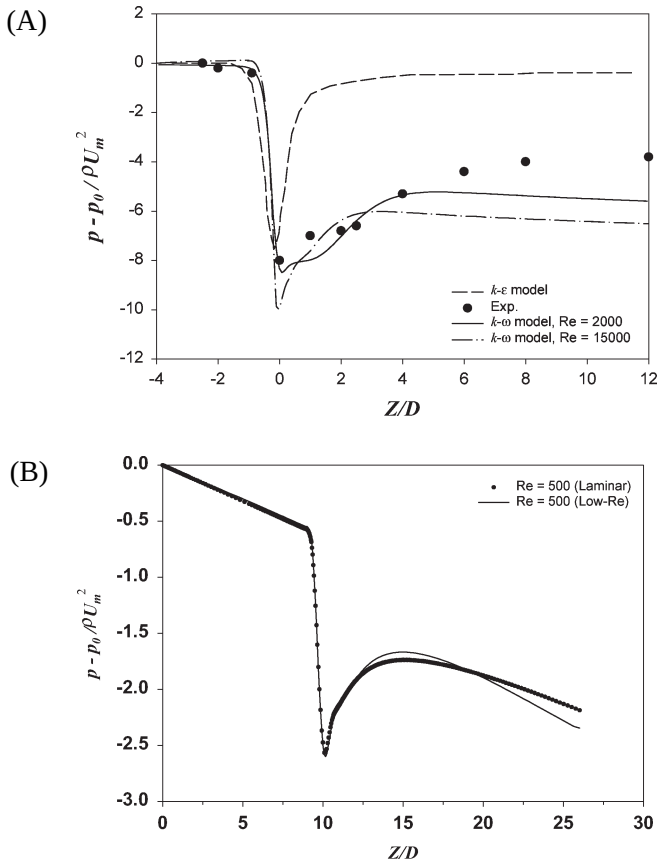

Fig. 6. Wall static pressure distributions. (A) Comparison of theoretical prediction by k-ω model and the standard k-ε model (Zijlema et al., 1995) with experimental measurements (Deshpande and Giddens, 1980); (B) Comparison of the low-*Re* turbulence model with the laminar flow model in a 50% stenosis at $Re = 500$.

of reported experimental measurements (Yongchareon and Young, 1979; Jones, 1985). The calculation shows that the critical Reynolds number for the third model with a 86% stenosis is approximately 230. Figure 5 shows this phenomenon by demonstrating that the vortex length for this level of stenosis passes through a maximum value between *Re* equal to 200 and 300.

The vortex length prediction by laminar flow modeling has also been plotted in Fig. 4 for comparison. The figure shows that in the laminar flow range, the vortex length prediction by the present low-*Re* turbulence model is in good agreement with that obtained by laminar flow modeling. However, the laminar flow model overestimates the vortex length when the flow becomes transitional or turbulent.

3.3. Pressure distribution

Figure 6A presents the distribution of the calculated wall static pressure for Model 2 at a *Re* of 2,000. For comparison, the experimental measurements (Deshpande and Giddens, 1980) and the theoretical calculation from the k-ε model (Zijlema et al., 1995) at $Re = 15{,}000$ are

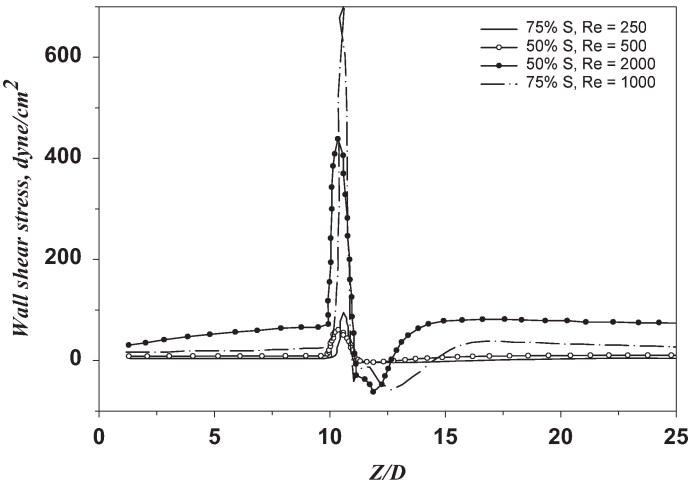

Fig. 7. Wall shear stress distributions.

plotted in the same figure. It can be seen that the wall static pressure distribution predicted by the present model is consistent with the experimental measurements, both in the acceleration flow zone and the deceleration area of the flow. On the other hand, the k-ε model gives a more rapid and much higher pressure recovery prediction in the deceleration zone. The results of wall pressure drop calculated by low-*Re* model at $Re = 15{,}000$ are also included in Fig. 6A for comparison.

The predicted wall static pressure distribution in Model 1 for $Re = 500$ is plotted in Fig. 6B and is compared to the results obtained by laminar-flow modeling. The two sets of data are remarkably similar, indicating that the present low-*Re* turbulence model provides a good prediction of pressure, even in the case of laminar flow.

3.4. Wall shear stress

Figure 7 shows the distribution of wall shear stress as a function of distance from the throat of the stenosis for Models 1 and 2 at different values of *Re*. The highest and the lowest absolute values of wall shear stress appear at the throat of the stenosis and at the reattachment point of the vortex, respectively. In the vortex region, wall shear rates assume negative values, indicating that wall shear stresses are acting in opposite directions upstream and downstream of the reattachment point.

The calculation reveals a distinctive difference in wall shear stress distribution between laminar flow and transitional or turbulent flow. When the flow is laminar, the wall shear stress recovers from the negative value downstream of the reattachment point, approaching, but never exceeding, the value found in a fully-developed Poiseuille flow. However, as the flow becomes transitional or turbulent, immediately downstream of the reattachment point, the wall shear stress jumps to a value higher than found in a fully-developed Poiseuille flow. It then decreases and approaches the Poiseuille-flow value farther downstream, indicating that the flow has resumed its laminar-flow state. This shows that the low-*Re* k-ω model is also capable of predicting relaminarization, a previously undocumented feature of the model.

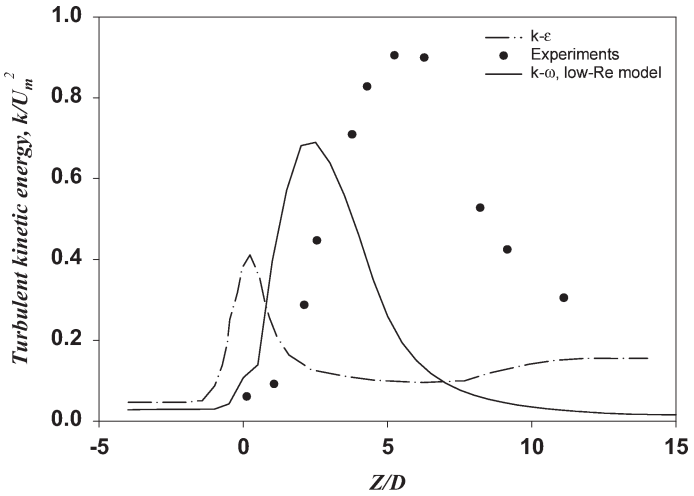

Fig. 8. Comparison of turbulence intensity distributions along the center line obtained from k-ω and k-ε models. The experimental data originated from Deshpande and Giddens (1980). The k-ε prediction originated from Zijlema et al. (1995).

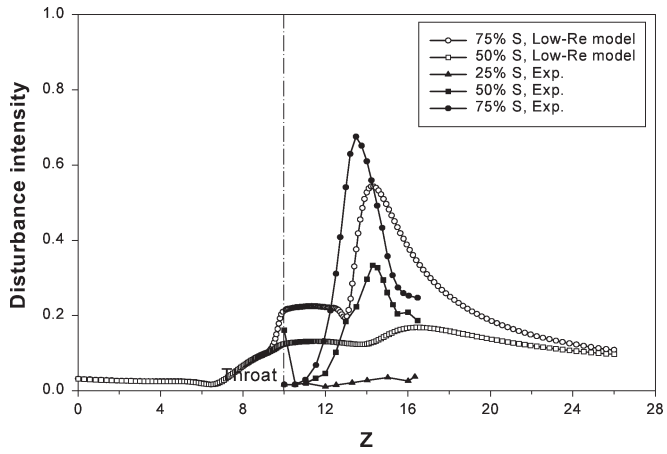

Fig. 9. Axial variations of center line disturbance intensities at $Re = 2000$ for different stenoses. Comparison of, the k-ω model predictions (Low-*Re* model) with experimental results (Exp.) from Saad and Giddens (1983).

3.5. Turbulence intensity along the center line

Figure 8 shows the profile of the turbulence intensity along the center line for Model 2 at a Reynolds number of 2000. For comparison, the equivalent experimental measurements (Deshpande and Giddens, 1980) and calculations obtained from the k-ε model (Zijlema et al., 1995) at $Re = 15{,}000$ are presented in the same figure. The comparison shows that the k-ε turbulence model gives a poor prediction of center line turbulence. On the other hand the present low-*Re* model does predict that the turbulent intensity increases after the throat and

reaches a peak at the vortex center in the flow separation zone. Although there are significant differences between the predicted and experimental data, the predicted turbulence intensity distribution is qualitatively similar to that presented by the experimental measurements, confirming that the low-*Re* model is better suited than the k-ε model for predicted flow in arterial stenoses. Figure 9 provides a comparison of disturbance intensities at various degrees of stenosis along the center line for $Re = 2000$.

4. Discussion

Under physiological conditions, blood flow may remain laminar proximal (upstream) to moderate and severe stenoses but becomes transitional or turbulent distally (Clark, 1976; Cassanova and Giddens, 1978; Saad and Giddens, 1983). Experimental studies have shown that the critical Reynolds number at which flow becomes transitional or turbulent in a stenosis is a function of its severity, being 1,100 for a 50% stenosis and 400 for a 75% stenosis (Yongchareon and Young, 1979; Jones, 1985).

In the past, most numerical modeling of stenotic flow has been limited to a laminar flow approach (Lee and Fung, 1970; Daly, 1976; Deshpande et al., 1976), which provides incorrect hemodynamic information and is of limited benefit to research on hemodynamic-related vascular disorders. For instance, laminar flow modeling usually underestimates shear stresses and pressure loss through an arterial stenosis if transitional/turbulent flow occurs distal to the stenosis. Clearly laminar flow modeling cannot provide flow information such as turbulent kinetic energy and turbulence spectrum in the transitional/turbulent flow region. Turbulence has a profound impact on blood vessel walls. For example, flow turbulence may induce the arterial wall to vibrate (Boughner and Roach, 1971; Roach, 1972) and may directly lead to adaptive morphological changes in the arterial wall such as intimal hyperplasia (Cassanov and Giddens, 1978). Turbulent shear stresses are also more damaging to blood cells than stresses associated with laminar or molecular shear stress (Hellumus and Brown, 1977).

Realizing that turbulent blood flow may occur in arterial stenoses, Deshpande (1977) employed a turbulence model to simulate the blood flow in arterial stenoses. Assuming laminar flow below a Reynolds number of 2,000, he carried out turbulence modeling at high Reynolds numbers, with most predictions assuming *Re* to be as high as 15,000, which is certainly unrealistic for the circulatory system.

Since the time-average Reynolds number is approximately 1,500 for the human ascending aorta and 400 for the human carotid artery, the realistic approach to flow simulation of arterial stenoses should be to assume that the proximal flow is laminar and the distal flow is transitional or turbulent with a low Reynolds number. To address these conditions, we have used Wilcox low-*Re* k-ω turbulence model to predict arterial stenotic flow. We have compared the results obtained with this low-*Re* model with previous experimental measurements as well as with results obtained by the standard k-ε model in terms of velocity profile, vortex length, wall shear stress, wall static pressure, and turbulence intensity.

The comparisons show that the results predicted by the low-*Re* model are in good agreement with reported experimental data. Using this model, we have accurately predicted the critical Reynolds number at which blood flow becomes transitional or turbulent distal to a stenosis. More interestingly, we have found that in the laminar flow region, the vortex length predicted

by this model also matches the vortex length predicted by the laminar flow method. This suggests that the low-*Re* model is not only suitable for the prediction of low Reynolds number transitional or turbulence stenotic flow, but also for laminar flow modeling distal to a stenosis. To further verify this, we have compared the wall static pressure prediction in a 50% stenosis at *Re* of 500 with the results obtained by laminar flow modeling. The comparison confirms that the low-*Re* k-ω model may indeed also be used for studying laminar flow (Fig. 6B).

In terms of wall static pressure and turbulence intensity, the low-*Re* k-ω turbulence model appears to give more accurate predictions than the standard k-ε model. In this study we found that both the wall pressure and turbulence intensity predicted by the low-*Re* k-ω model are very similar to the experimental measurements, while on the other hand the k-ε model predicts too rapid and excessive pressure recovery in the deceleration zone as well as giving poor prediction of turbulence intensity.

5. Conclusion

The predictions of arterial stenotic flow obtained with the Wilcox low-*Re* k-ω turbulence model have been found to be in good agreement with experimental measurements over the range of physiologically relevant Reynolds numbers. The low-*Re* k-ω turbulence model can therefore provide satisfactory information regarding blood flow in arterial stenoses, which is difficult to obtain accurately by experimental methods or by laminar-flow modeling. Most importantly, we have demonstrated that the proposed model is suitable for blood flow studies in certain areas of the arterial tree where both laminar and transitional/turbulent flows coexist.

Acknowledgement

This work has been supported by the Québec Biomaterials Institute.

References

Boughner DR, Roach MR. Effect of low frequency vibration on the arterial wall. Circ. Res., 1971; 29:136–144.

Cassanova RA, Giddens DP. Disorder distal to modeled stenoses in steady and pulsatile flow. J. Biomech., 1978;11:441–453.

Clark C. Turbulent velocity measurements in a model of aortic stenosis. J. Biomech., 1976;9:677–687.

Clark C. The propagation of turbulence produced by a stenosis. J. Biomech., 1980;13:591–604.

Daly BJ. A numerical study of pulsatile flow through stenosed canine femoral arteries. J. Biomech., 1976;9:465–475.

Deshpande MD, Mabon RF, Giddens DP. Steady laminar flow through modelled vascular stenoses. J. Biomech., 1976;9:165–174.

Deshpande MD. Steady laminar and turbulent flow through vascular stenoses models. Ph.D. Thesis, Georgia Institute of Technology; 1977.

Deshpande MD, Giddens DP. Turbulence measurements in a constricted tube. J. Fluid Mech., 1980; 97:65–89.

FIDAP Tutorial Manual. Fluid Dynamics Analysis Package; 1995. pp. 7–13.

FIDAP Update Manual. Fluid Dynamics Analysis Package; 1995. pp. 3–13.

Giddens DP, Mabon RF, Cassanova RA. Measurements of disordered flows distal to subtotal vascular stenoses in the thoracic aortas of dogs. Circ. Res., 1976;39:112–119.

Hellums JD, Brown CH. Blood cell damage by mechanical forces. In: Cardiovascular Flow Dymanics and Measurements. Hwang HC, Normann A, Eds, Baltimore University: Park Press; 1977. pp. 799–823.

Jones SA. A study of flow downstream of a constriction in a cylindrical tube at low Reynolds numbers with emphasis on frequency correlations. Ph.D. Thesis, University of California; 1985.

Lee JS, Fung YC. Flow in locally constricted tubes at low Reynolds numbers. J. Appl. Mech., 1970;37:9–16.

Roach MR. Poststenotic dilatation in arteries. Cardiovascular Fluid Dynamics, 1972;2:111–139.

Saad AA, Giddens DP. Velocity measurements in steady flow through axisymmetric stenoses at moderate Reynolds numbers. J. Biomech., 1983;16:505–516.

Strandness DE JR., Didisheim P, Clowes AW, Watson JT., Eds. Vascular Disease–Current Research and Clinical Applications. Orlando, USA: Grune and Stratton; 1987.

Wilcox DC. Turbulence Modeling in CFD. La Canada California: DCW Industries; 1993.

Yongchareon W, Young DF. Initiation of turbulence in models of arterial stenoses. J. Biomech., 1979;12:185–196.

Zijlema M, Segal A, Wesselinh P. Finite volume computation of 2D incompressible turbulent flows in general coordinates on staggered grids. Int. J. Numer. Methods in Fluids, 1995;20:621–640.